




RESEARCH ARTICLE | SEPTEMBER 13 2023

Design and experimental verification of the working mode of an electrostatic suspension accelerometer

Zuolei Wang ; Yunpeng Li; Jungang Lei; Zhenxing Wang; Dongxue Xi; Jian Min; Yongqiang Wei; Shijia Yang ; Ziren Luo 

 Check for updates

AIP Advances 13, 095014 (2023)

<https://doi.org/10.1063/5.0164294>



View Online



Export Citation

08 April 2024 03:54:24

AIP Advances

Why Publish With Us?



25 DAYS
average time
to 1st decision



740+ DOWNLOADS
average per article



INCLUSIVE
scope

[Learn More](#)

 AIP Publishing

Design and experimental verification of the working mode of an electrostatic suspension accelerometer

Cite as: AIP Advances 13, 095014 (2023); doi: 10.1063/5.0164294

Submitted: 22 June 2023 • Accepted: 21 August 2023 •

Published Online: 13 September 2023



View Online



Export Citation



CrossMark

Zuolei Wang,^{1,a)}  Yunpeng Li,¹ Jungang Lei,¹ Zhenxing Wang,² Dongxue Xi,¹ Jian Min,¹ Yongqiang Wei,¹ Shijia Yang,¹  and Ziren Luo³ 

AFFILIATIONS

¹Lanzhou Institute of Physics, China Academy of Space Technology (CAST), Lanzhou, China

²Institute of Remote Sensing Satellite, China Academy of Space Technology (CAST), Beijing, China

³Institute of Mechanics, Chinese Academy of Sciences (CAS), Beijing, China

^{a)}Author to whom correspondence should be addressed: wzlgam2000@163.com

ABSTRACT

An electrostatic suspension accelerometer is an important instrument for measuring quasi-steady micro-acceleration. A reasonable working mode is the premise to ensure acquisition and stable control of the accelerometer in-orbit and then to carry out high-precision linear measurement. Based on the dynamic model analysis of the electrostatic suspension accelerometer, and taking the force balance of inertial proof mass as the fundamental requirement, the design of the acquisition working mode and measurement working mode based on displacement sensing output and feedback control output is proposed. The rationality and feasibility of the proposed working mode design are verified by the ground drop tower test of the Taiji-1 accelerometer prototype and in-flight test of the actual product.

© 2023 Author(s). All article content, except where otherwise noted, is licensed under a Creative Commons Attribution (CC BY) license (<http://creativecommons.org/licenses/by/4.0/>). <https://doi.org/10.1063/5.0164294>

I. INTRODUCTION

The electrostatic suspension accelerometer (ESA) works based on the principle of differential capacitance detection and electrostatic force servo feedback control. It achieves precise measurement of quasi-steady micro-acceleration by measuring the electrostatic force required to maintain proof mass (PM) at the center of an electrode cage.¹ The weight of PM is set from dozens of grams to hundreds of grams, the average spacing between the electrode and PM is set from dozens of micrometers to hundreds of micrometers, and the polarization voltage and the feedback control voltage is set from a few volts to hundreds of volts so as to realize different ranges and resolutions to meet different task requirements. The typical frequency bandwidth of the ESA is 10^{-4} to 0.1 Hz, the range is 10^{-7} to 10^{-2} m/s², and the resolution is 10^{-12} to 10^{-8} m s⁻² Hz^{-1/2}. It is mainly used for measuring atmospheric drag, solar radiation pressure, gravity gradient, and micro-vibration on satellites^{2,3} and has important applications in satellite gravity

measurement, satellite precision orbit determination, autonomous navigation, space microgravity measurement, and space gravitational wave detection.^{4,5}

Although the average spacing of the ESA sometimes reaches millimeters, PM needs to avoid contact with the electrodes to prevent short circuit and adapt to the mechanical vibration environment at the launch stage. Therefore, the motion range of PM is usually limited by mechanical stops or directly locked by a dedicated mechanism and then released in orbit.⁶ Since the ESA works in closed-loop servo feedback control mode, PM needs to be controlled at the center of the electrode cage. PM usually deviates significantly from the center of electrodes during the ESA's initial start-up, and it is necessary to be acquired and controlled at the center of the electrode by electrostatic force first. In addition, different measurement ranges are usually needed to ensure that the ESA can adapt to the complex micro-vibration conditions in orbit. Therefore, the design of the working mode is an important part of ESA scheme design, which is directly related to whether it operates normally.

The ESA was first developed by NASA in the United States and matured by ONERA in France.^{7,8} However, there have been no reports on how to design the working mode of the ESA.⁹⁻¹² Based on the working principle of the ESA, the design of the working mode is introduced in this paper to ensure acquisition and high-precision linear measurement. In addition, the ground and flight test results of a typical ESA verify the rationality of its working mode design.

II. WORKING MODE DESIGN

A. Dynamic model analysis

Figure 1 shows the force schematic on PM of the ESA. Relative displacement will occur between the PM and the electrode on non-gravitational acceleration input. The differential capacitance formed due the deviation of the PM from the electrode center is detected by the sensing circuit, and the corresponding feedback control voltage will be applied to the electrode through the proportion integra differentiation (PID) controller calculation. The electrostatic force generated by the feedback control voltage makes the PM follow the electrode frame. The feedback control voltage is proportional to the input acceleration so as to achieve precise measurement of the input acceleration.

Assume that the upward direction shown Fig. 1 is positive. The motion equations of the electrode frame and PM are expressed respectively, as

$$x_f'' = -a_{in}, \tag{1}$$

$$x_m'' = -a_e = -F_e/m, \tag{2}$$

where x_f is the displacement of the electrode frame, x_m is the displacement of PM relative to the earth's inertial coordinate system, a_{in} is the acceleration of the non-conservative force on the satellite (electrode frame) in the earth inertial coordinate system, a_e is the acceleration of the PM due to the electrostatic force F_e , and m is the weight of the proof mass,

$$x_m - x_f = x, \tag{3}$$

$$F_e = mG_P V_f + m\omega_p^2 x, \tag{4}$$

where x is the displacement of PM from the electrode center and G_P is the physical feedback coefficient between the feedback control voltage and the electrostatic force acceleration,

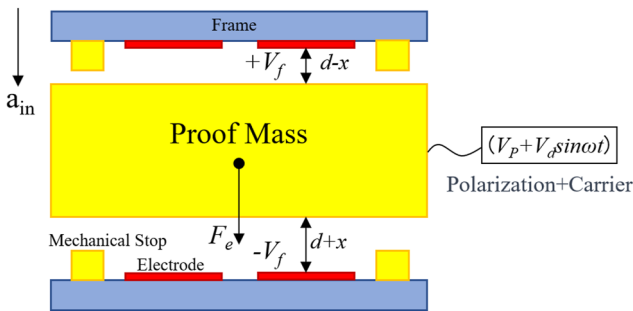


FIG. 1. Schematic of the force on PM.

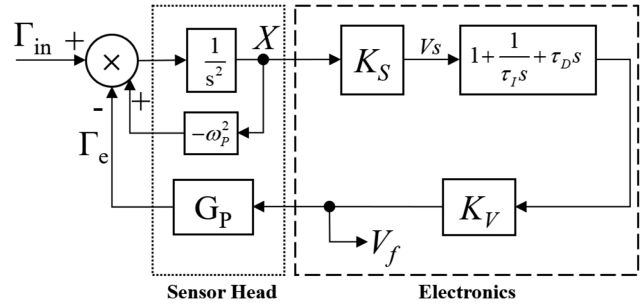


FIG. 2. Closed-loop control block diagram of the ESA.

$$G_P = \frac{2\epsilon_0 A V_P}{m d^2}, \tag{5}$$

where ϵ_0 is the vacuum dielectric constant, A is the electrode area, d is the average spacing between the PM and the electrode, and V_P is the DC polarization voltage applied to the PM. V_f is the feedback control voltage applied to the electrode,

$$V_f = K_S K_V \left(x(t) + \frac{1}{\tau_I} \int_0^t x(t) dt + \tau_D x'(t) \right), \tag{6}$$

where K_S is the displacement detection gain, K_V is the feedback acting gain, and τ_I and τ_D are the integral and differential time constants of the PID controller, respectively. ω_p is the angular frequency associated with the electrostatic negative stiffness,

$$\omega_p^2 = -\frac{2\epsilon_0 A}{m d^3} (V_P^2 + V_{dms}^2 + V_f^2), \tag{7}$$

where V_{dms} is the effective value of the high-frequency carrier applied to the PM.

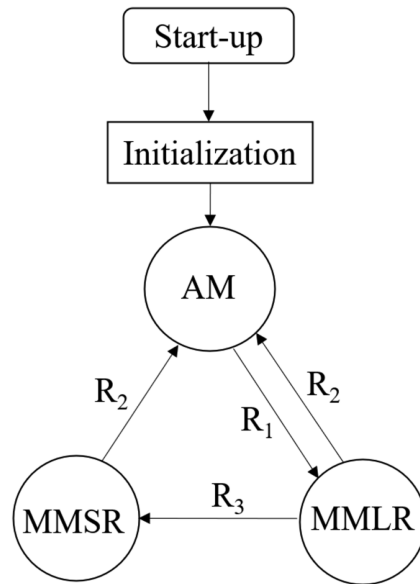


FIG. 3. Typical working mode design.

TABLE I. Conditions and criteria for working mode switching.

Conditions	Criterion	Note
R ₁	The sensing outputs of all channels in a judgment period T ₁ : V _s ≤ V _{sa}	V _{sa} = K _{Sa} x _{mm}
R ₂	The sensing output of any channel in a judgment period T ₂ : V _s ≥ V _{sma}	V _{sma} = 0.9V _{sm}
R ₃	The sensing output of all channels in a judgment period T ₃ : V _s ≤ V _{smls} ; the feedback voltage of all channels: V _f ≤ V _{fmls}	V _{smls} = 0.5V _{sm} V _{fmls} = 0.9 $\frac{V_{Pms}}{V_{Pml}}$ V _{fms}

TABLE II. Electrode and electronic parameters of the Taiji-1 ESA.

	Parameter	Design value	Unit
Sensor head	Weight of PM	72	g
	Average electrode spacing of the sensitive axis in the horizontal direction: d _Y , d _Z	75, 75	μm
	Average electrode spacing of the non-sensitive axis in the vertical direction: d _X	60	μm
	Electrode area of the sensitive axis: A _Y , A _{Z1} , A _{Z2}	2, 1, 1	cm ²
	Electrode area of the non-sensitive axis: A _{X1} , A _{X2} , A _{X3}	5, 2.5, 2.5	cm ²
	Average free-motion range of the PM relative to the electrode center limited by the mechanical stop in the sensitive axis	±20	μm
Electronic	Average free-motion range of the PM relative to the electrode center limited by the mechanical stop in the non-sensitive axis	±12	μm
	Polarization voltage V _P in AM and MM	20, 5	V
	Carrier voltage V _{d-rms} in AM and MM	1, 4	V
	Maximum feedback voltage V _{fm} in AM and MM	±17.5, ±10	V
	Maximum input voltage V _{sm} of the controller	±2.5	V

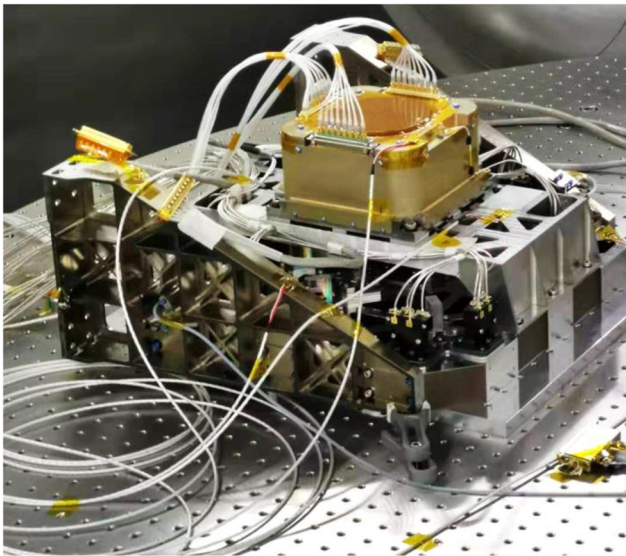


FIG. 4. Photo of the Taiji-1 ESA sensor head in the ground test.

It can be obtained from Eqs. (1)–(3) that

$$x'' = a_{in} - G_P V_f - \omega_p^2 x. \tag{8}$$

Furthermore, we get

$$\begin{aligned} a_{in} &= x'' + G_P K_s K_V \left(x + \frac{1}{\tau_I} \int_0^t x d\tau + \tau_D x' \right) + \omega_p^2 x \\ &= x'' + (\omega_0^2 + \omega_p^2) x + \omega_0^2 \tau_D x' + \frac{\omega_0^2}{\tau_I} \int_0^t x d\tau. \end{aligned} \tag{9}$$

In the above-mentioned equation, ω₀ represents the natural angular frequency of the system,

$$\omega_0^2 = k_S k_V G_P. \tag{10}$$

From Eq. (9), it can be seen that the ESA can also be regarded as a spring-mass oscillator system,¹³ where (ω₀² + ω_p²) is the system stiffness and ω₀²τ_D is the system damping coefficient. In order to ensure the stability of the ESA, (ω₀² + ω_p²) must be greater than zero to ensure that it is a positive stiffness system. Since ω_p is negative stiffness, ω₀² > |ω_p²| is required. The larger the system stiffness, the faster the response, and the better the robustness.

Figure 2 shows the closed-loop control block diagram of the ESA. The transfer function of the measured electrostatic force acceleration Γ_e relative to the input acceleration Γ_{in} is

$$\frac{\Gamma_e(s)}{\Gamma_{in}(s)} = \frac{H(s)}{1 + \omega_p^2 s + H(s)}, \quad (11)$$

where s is the Laplace operator,

$$H(s) = \omega_0^2 \left(1 + \frac{1}{\tau_I s} + \tau_D s \right). \quad (12)$$

When ESA reaches system steady control, $s \rightarrow 0$; then,

$$\Gamma_e = \Gamma_{in}. \quad (13)$$

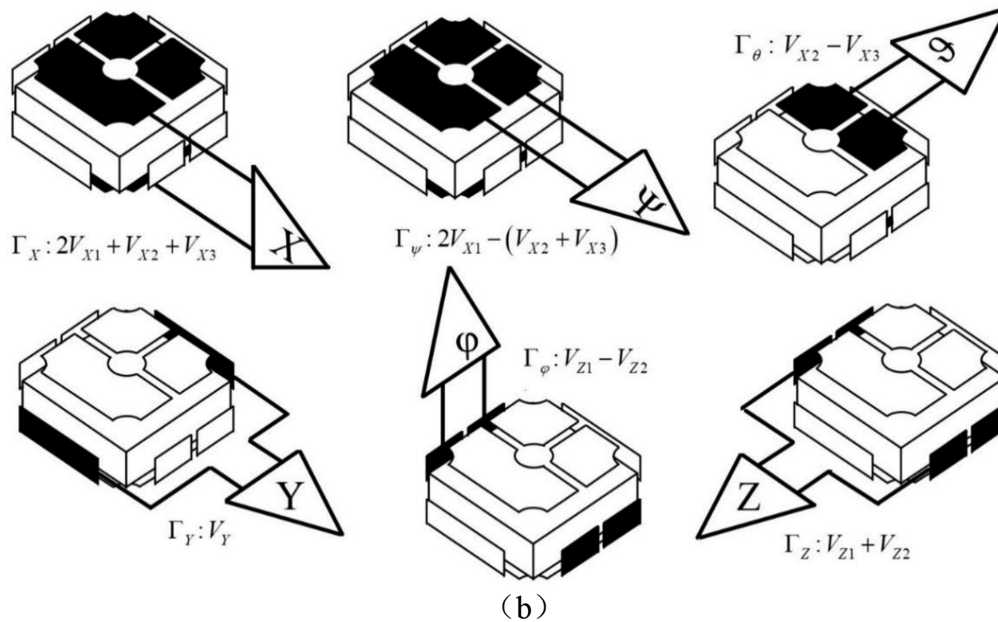
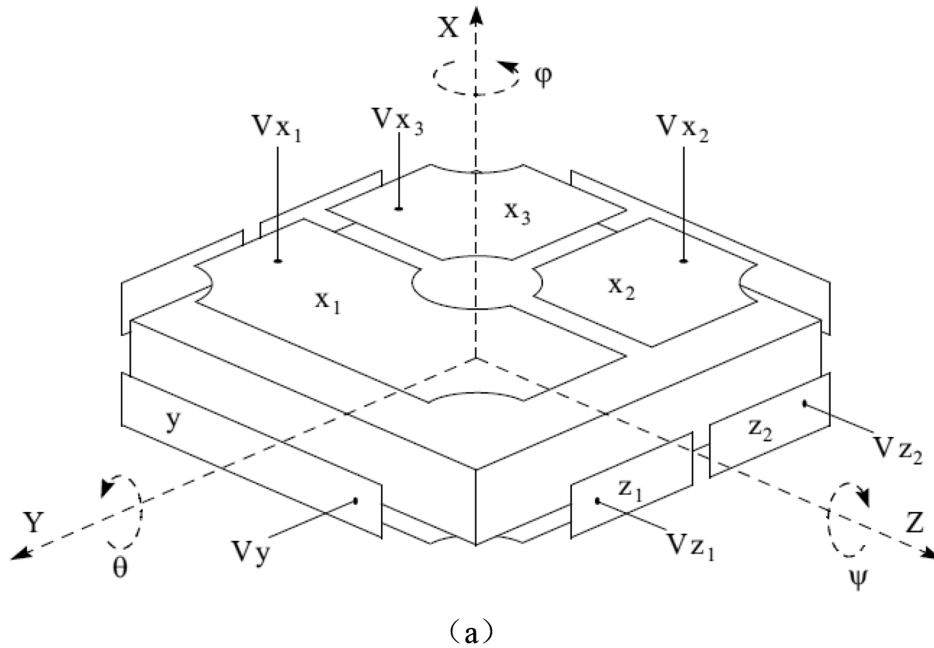


FIG. 5. Electrode configuration scheme and signal combination of the ESA: (a) Electrode configuration scheme. (b) Six-degree-of-freedom signal detection and control.¹⁵

TABLE III. Electronic parameters design of the four working modes of the Taiji-1 ESA prototype in the drop tower test.

Working mode	V_p (V)	V_{fm} (V)	V_{d-rms} (V)	V_{sm} (V)
AM-1	53	± 34	1	± 2.5
MM-1	20	± 17.5	4	± 2.5
AM-2	20	± 17.5	1	± 2.5
MM-2	5	± 10	4	± 2.5

Therefore, the ESA can accurately measure the acceleration signal whose change period is below its system response time. Regardless of the system bias and noise, the input acceleration is expressed by the electrostatic force acceleration,

$$a_{in} = a_e = G_p V_f. \tag{14}$$

B. A typical working mode design

An ESA is typically designed with two working modes: acquisition mode (AM) and scientific measurement mode (MM).⁹ AM is

designed to provide a larger electrostatic force to acquire and control PM from its initial position to the center of the electrode cage. In AM, the ESA has a wider range of position sensing for PM and lower system stiffness, allowing for smooth acquisition of PM over a long time to prevent the electrode from being damaged by overshoot. MM corresponds to the case where PM is controlled near the center of the electrode cage. The system stiffness in MM is larger, and the ESA can achieve faster response to the input signal and higher linearity measurement. In order to ensure that the ESA adapts to complex micro-vibrations in orbit and achieves optimal measurement performance, MM may be further designed into a large range (MMLR) and a small range (MMSR).

The carrier voltage amplitude, polarization voltage, and maximum feedback voltage in the three working modes usually satisfy the following relationship:

- Carrier voltage: $V_{dm} > V_{da}$
- Polarization voltage: $V_{pa} > V_{pml} > V_{pms}$
- Maximum feedback voltage $V_{fa} > V_{fml} > V_{fms}$.

Here, V_{da} is the carrier voltage in AM, V_{dm} is the carrier voltage in measurement mode, V_{pa} is the polarization voltage in acquisition mode, V_{pml} is the polarization voltage in

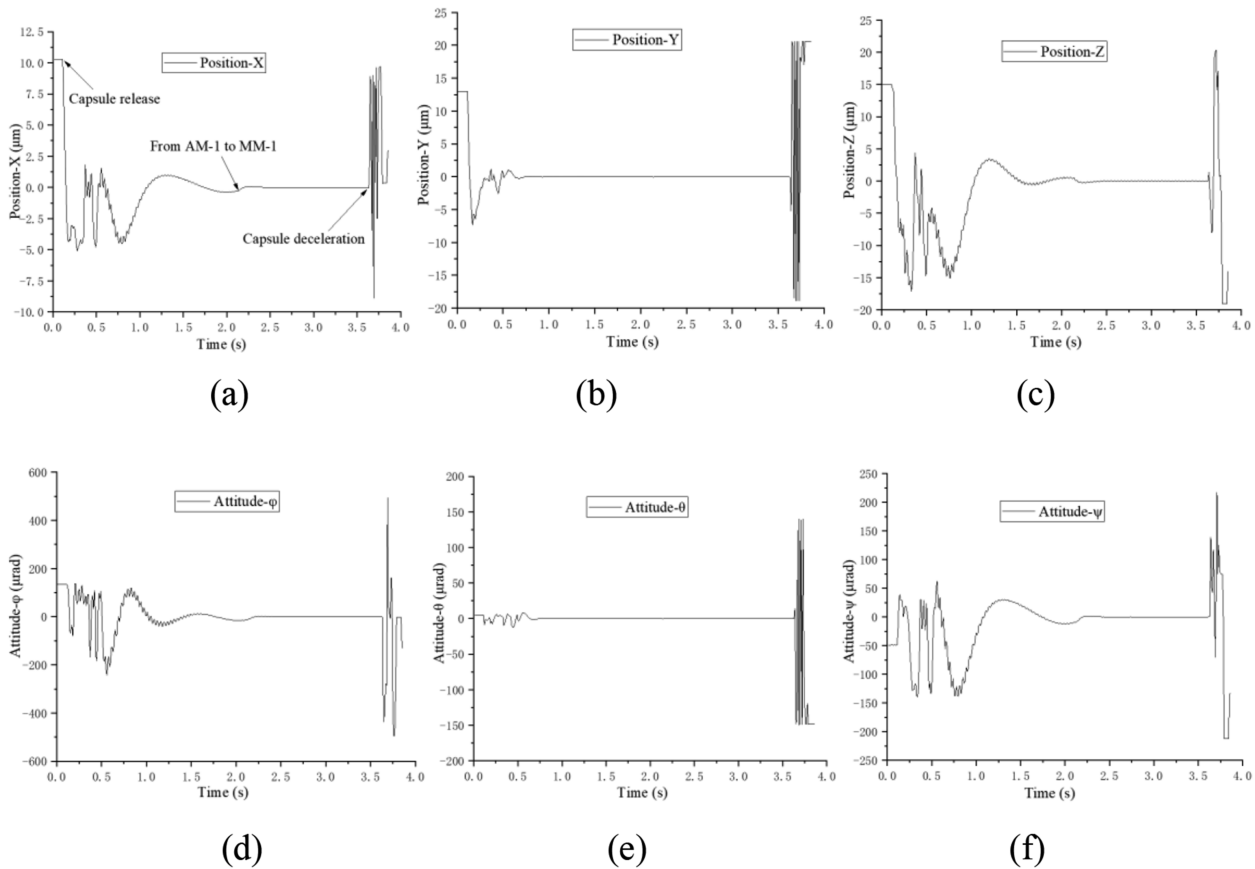


FIG. 6. Position and attitude acquisition process of the TM in the first drop tower test of the Taiji-1 ESA prototype: (a) X-axis acquisition. (b) Y-axis acquisition. (c) Z-axis acquisition. (d) ϕ -attitude acquisition. (e) θ -attitude acquisition. (f) ψ -attitude acquisition.

08 April 2024 03:54:24

measurement mode with a large range, V_{pms} is the polarization voltage in measurement mode with a small range, V_{fa} is the maximum feedback voltage in acquisition mode, V_{fml} is the maximum feedback voltage in measurement mode with a large range, and V_{fms} is the maximum feedback voltage in measurement mode with a small range.

The range x_m of position identification of the ESA to PM is determined by the detection gain K_s and the maximum input voltage V_{sm} of the controller,

$$x_m = V_{sm}/K_s. \quad (15)$$

For a certain controller, the input and output range of the controller are limited by hardware and cannot be changed. The only adjustable parameter is the detection gain K_s .

The displacement sensing output V_s of the ESA, which corresponds to the input of the controller, is expressed by the following equation:

$$V_s = \frac{\Delta C}{C_f} V_{drms} K_C, \quad (16)$$

where $\frac{\Delta C}{C_f} V_{drms}$ represents the sensing output of the capacitance bridge, C_f is the feedback capacitance of the charge amplifier, and K_C is the AC amplification factor from the capacitance bridge to the controller. ΔC is the differential capacitance formed by the deviation of PM from the electrode center,

$$\Delta C = \frac{2\epsilon_0 A x}{d^2 - x^2}. \quad (17)$$

Since the motion range of PM is restricted by the mechanical stops, the displacement x of PM that deviates from the center of the electrode center is much smaller than the average distance d of the electrode, with $x \ll d$. Then,

$$\Delta C = \frac{2\epsilon_0 A x}{d^2}, \quad (18)$$

$$V_s = \frac{2\epsilon_0 A}{d^2 C_f} V_{drms} K_C x. \quad (19)$$

Therefore, the gain of displacement sensing is expressed by the following equation:

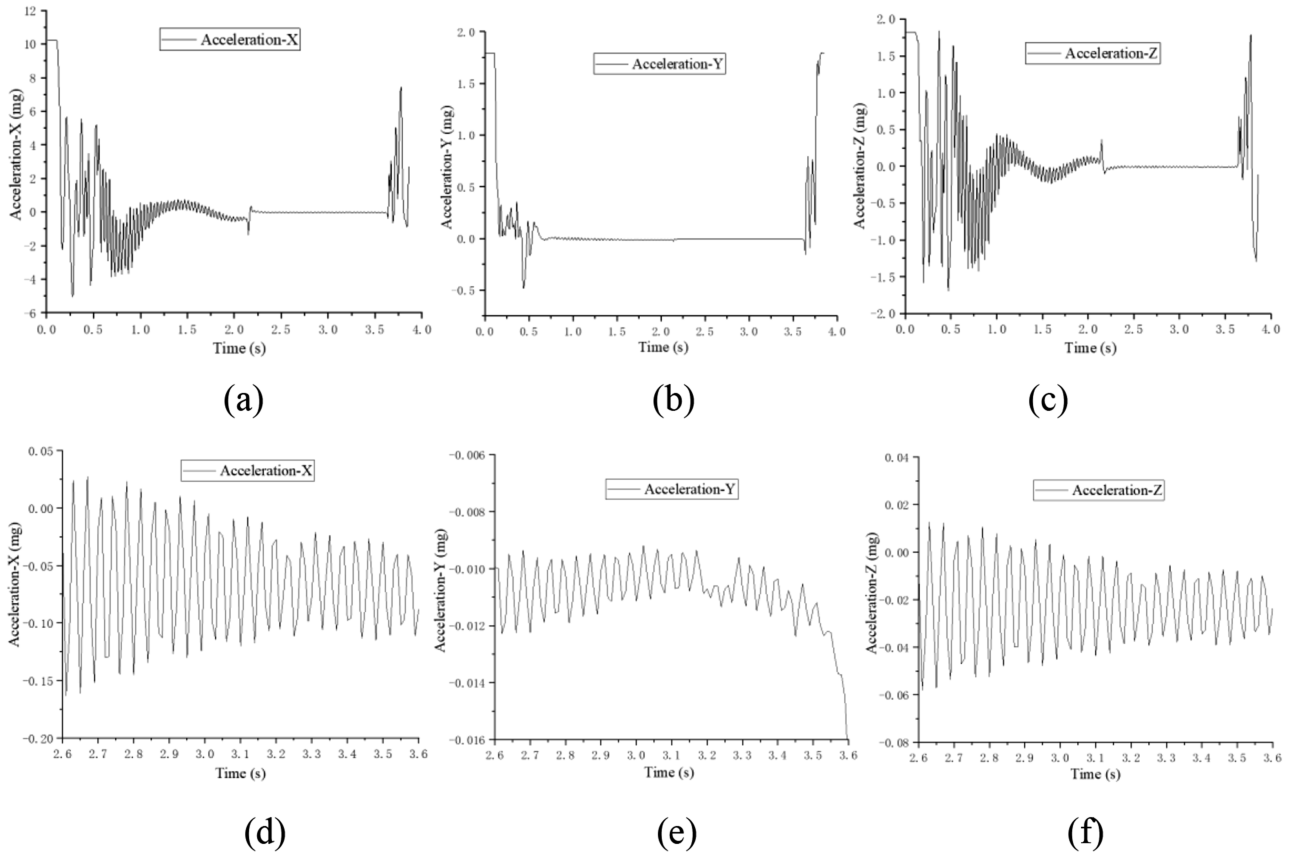


FIG. 7. Microgravity acceleration of the capsule in the first drop tower test: (a) X-axis acceleration. (b) Y-axis acceleration. (c) Z-axis acceleration. (d) X-axis acceleration in final 1 s. (e) Y-axis acceleration in final 1 s. (f) Z-axis acceleration in final 1 s.

$$K_S = \frac{2\epsilon_0 A}{d^2 C_f} V_{drms} K_C. \quad (20)$$

$$V_S = \frac{2\epsilon_0 A}{d^2 C_f} V_{da-rms} K_C x_{am} = K_{Sa} x_{am} = V_{sm}, \quad (21)$$

From Eq. (20), the adjustment of detection gain can be achieved through the AC amplification factor K_C and the carrier amplitude V_{drms} . However, adjusting the AC amplification factor K_C will directly affect the output noise of displacement sensing. Moreover, AC amplification factors of six sensing channels at least need to be adjusted simultaneously to meet the six-degree-freedom sensing and control requirements if this adjustment method is adopted, which will greatly increase the system complexity. Since the carrier signal is applied to the PM, which serves as a common electrode, adjusting the amplitude of the carrier signal can simultaneously achieve the adjustment of the detection gain for all channels. This adjustment method can achieve the optimal signal-to-noise ratio of the capacitance bridge output, which is more feasible in technical and engineering implementation.

If the maximum displacement of PM that deviates from the center of the electrode is x_{am} , where the position of PM lies on the mechanical stop, then the carrier signal voltage V_{da} and detection gain in AM are usually designed as follows:

where V_{sm} is the maximum input voltage of the controller, V_{da-rms} is the root mean square of the carrier voltage in AM, and K_{sa} represents the displacement sensing gain in AM,

$$K_{Sa} = \frac{2\epsilon_0 A}{d^2 C_f} V_{da-rms} K_C. \quad (22)$$

In MM, the displacement identification range x_{mm} is usually designed according to the orthogonal error of the electrode and PM and combined with the maximum displacement of PM deviating from the center of the electrode when external acceleration is inputted. The value x_{mm} is usually much smaller than x_{am} to ensure high linearity of the measurement, and there is

$$V_S = \frac{2\epsilon_0 A}{d^2 C_f} V_{dm-rms} K_C x_{mm} = K_{Sm} x_{mm} = V_{sm}, \quad (23)$$

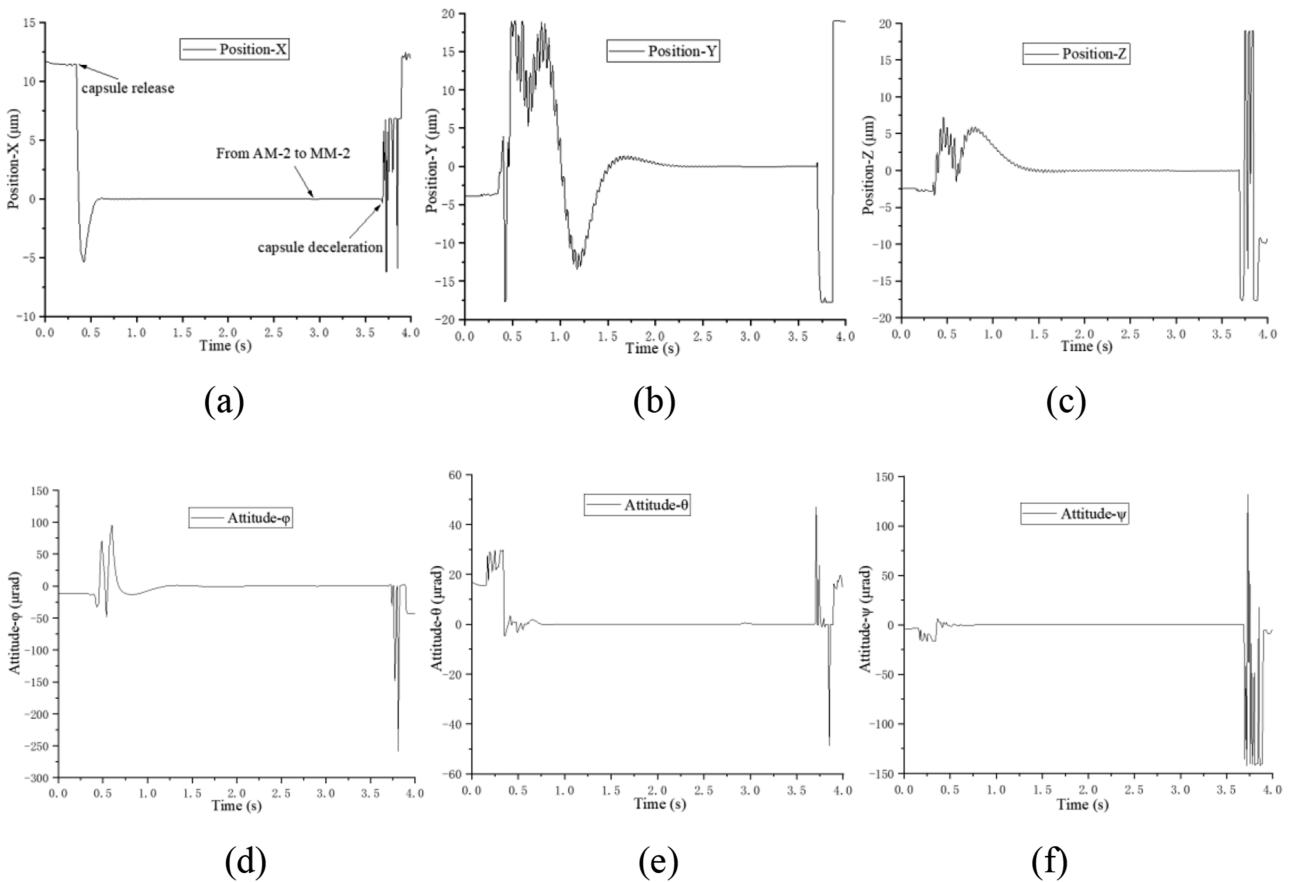


FIG. 8. Position and attitude acquisition process of the TM in the second drop tower test of the Taiji-1 ESA prototype: (a) X-axis acquisition. (b) Y-axis acquisition. (c) Z-axis acquisition. (d) ϕ -attitude acquisition. (e) θ -attitude acquisition. (f) ψ -attitude acquisition.

08 April 2024 03:54:24

where V_{dm-rms} is the root mean square of the carrier voltage in MM and K_{sm} represents the displacement sensing gain in MM,

$$K_{Sm} = \frac{2\epsilon_0 A}{d^2 C_f} V_{dm-rms} K_C. \quad (24)$$

According to Eq. (14), the maximum controllable measurement acceleration of the ESA is mainly determined by the bias voltage and the maximum feedback voltage, besides the electrode parameters. Therefore, the working mode of the ESA is mainly achieved by judging and adjusting the electronic parameters.

Figure 3 shows a typical working mode design of the ESA. PM is first controlled stably by AM and then transit to the MMLR. When the input acceleration enters the control range of the MMSR, the ESA will transit to the MMSR. Regardless of whether in the MMLR or MMSR, the ESA will transit to AM when the input acceleration exceeds the control range. Table I shows the switching conditions and criteria of various working modes. The threshold setting of the switching criteria is based on checking whether PM is stably controlled at the center of the electrode cage and whether the electrostatic force is sufficient to balance the input acceleration.

III. EXPERIMENTAL VERIFICATION OF THE ESA'S WORKING MODE

Taiji-1 is China's first experimental satellite for gravitational wave detection technology in space, and its main task is to carry out key technical verification such as laser metrology and drag-free control. An ESA is used as a key payload to provide a high-precision inertial reference for laser metrology and drag-free control.¹⁴ The main electrode parameters and electronic parameters of the ESA are shown in Table II. Based on the electrostatic force Eq. (4) and the parameters listed in Table II, the Taiji-1 ESA has an acquisition range of 189 and 1650 μg in the sensitive axis and non-sensitive axis, respectively, and the maximum controllable acceleration in MM is 45 and 341 μg , respectively. Figure 4 shows the ground experimental photo of the ESA sensor head. Figure 5 shows the electrode configuration scheme and the electrode signal combination designed to realize the six-degree-of-freedom signal detection and control. The common mode signal combination of the differential capacitance detection outputs and the feedback control outputs of different electrodes in the same axis provides the translational information of the PM, while the differential mode signal combination provides the rotational information. PM and the electrode cage form six pairs of differential capacitors in the three-axis direction so as to realize the

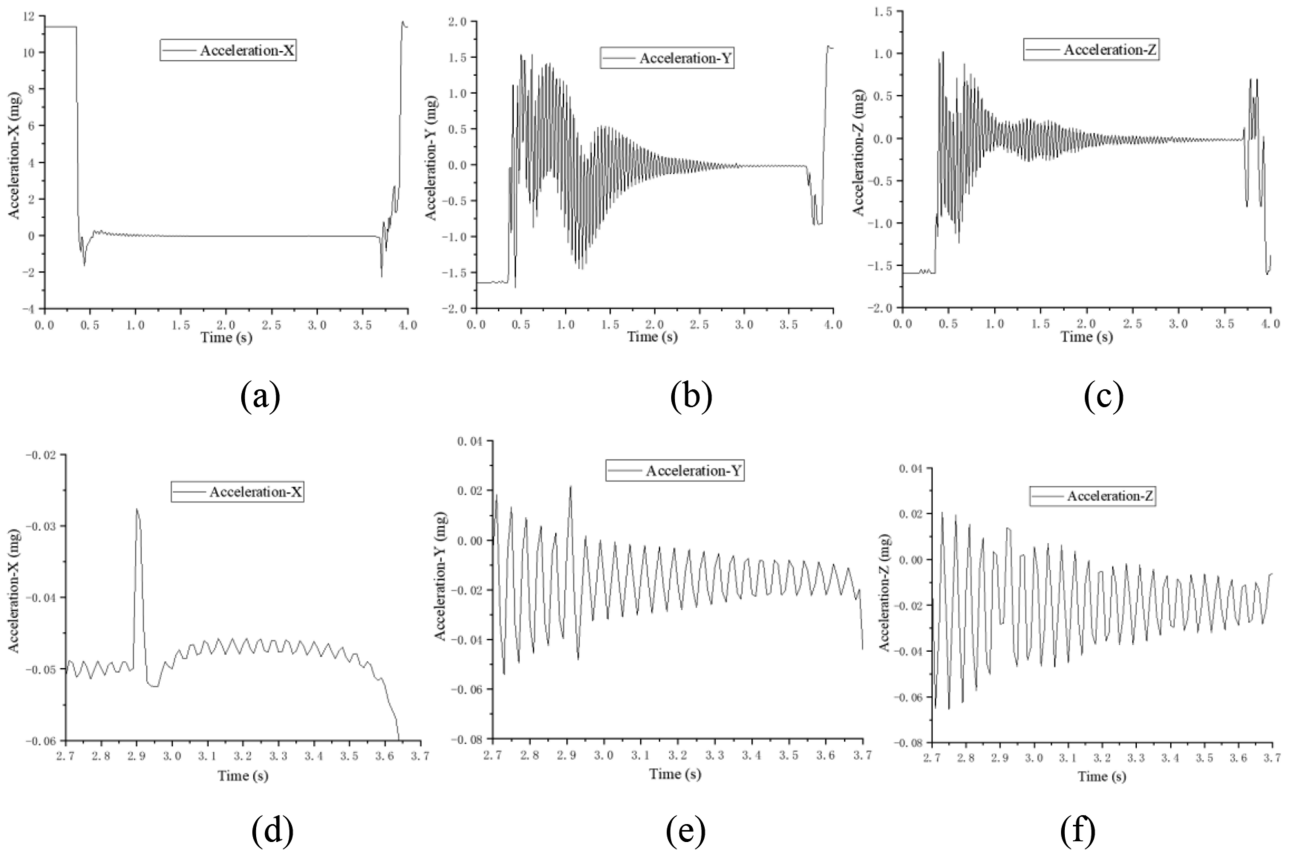


FIG. 9. Microgravity acceleration of the capsule in the second drop tower test: (a) X-axis acceleration. (b) Y-axis acceleration. (c) Z-axis acceleration. (d) X-axis acceleration in final 1 s. (e) Y-axis acceleration in final 1 s. (f) Z-axis acceleration in final 1 s.

sensing and control of the position and the attitude of PM. The Taiji-1 ESA is designed with two working modes in orbit: AM and MM. The working mode was verified by the ground test using an ESA prototype before launch. The drop tower test is the most representative test with respect to in-flight conditions. The main limitation of the drop tower test is the short free fall duration and microgravity level, so four working modes shown in Table III are adopted and two typical drop tower tests are carried out to verify the design rationality and control stability of the working mode design.

Considering that the free fall duration of the drop tower of NMLC is only about 3.5 s,¹⁶ in order to fully describe the acquisition and control of PM during free fall, the displacement sensing output and feedback drive data output rate are set to 100 sps when the Taiji-1 ESA prototype carries out the drop tower test. The judgment period T_1 of working mode switching is set to 1 s. The threshold V_{sa} of the sensing output voltage from AM to MM is set to 0.2 V, which ensures the displacement does not exceed 1 μm in the sensitive axis and 1.5 μm in the non-sensitive axis in a judgment period. Figure 6 shows the process from AM-1 transitioning to MM-1 listed in Table II during the first drop tower test. After the capsule was released for 2 s, the ESA prototype switched from

AM-1 to MM-1. This experiment verified the rationality of using displacement sensing output as the criterion for switching from AM to MM. The microgravity acceleration of the capsule in three directions was 20–100 μg , shown in Fig. 7, which is within the control range of the Taiji-1 ESA in orbit. Figure 8 shows the process from AM-2 to MM-2, listed in Table II, during the second drop tower test. After the capsule was released for 2.6 s, the ESA prototype switched from AM-2 to MM-2. The microgravity acceleration of the capsule in three directions was 5–20 μg , shown in Fig. 9. The design of working mode in orbit was verified through the second drop tower test. The control ability is stronger and the adjustment time is shorter in the first drop tower test than the second because the larger the bias voltage, and the larger the maximum feedback voltage of AM-1 relative to AM-2. It took about 2 s for AM-1 to transition to MM-1, while it took about 2.6 s for AM-2 to transit to MM-2.

Taiji-1 satellite was successfully launched on August 31, 2019.¹⁴ According to the verified working modes by the drop tower test on the ground, the ESA was successfully acquired and controlled in orbit, as shown in Fig. 10. It took about 2 s for AM to transition to MM, and then the non-gravitational acceleration in-orbit is

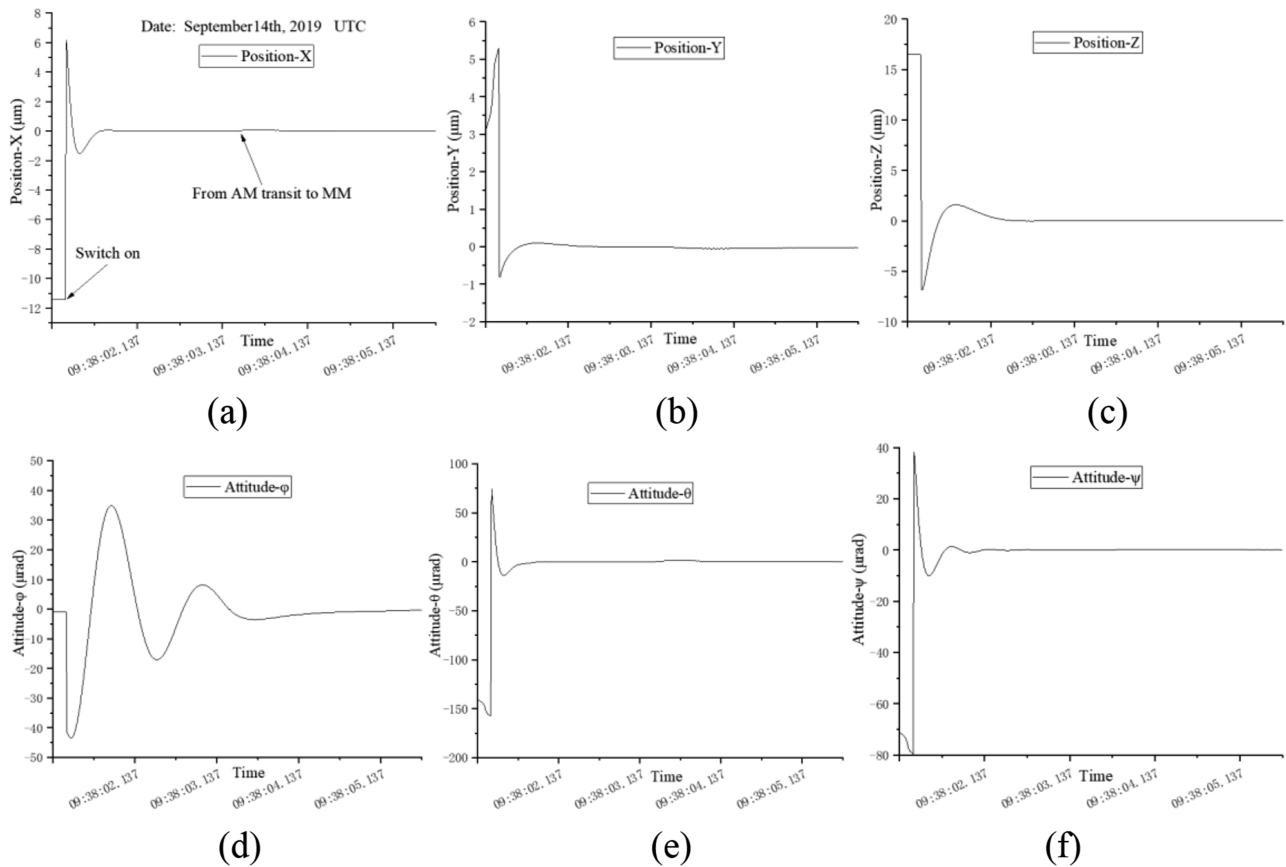


FIG. 10. Acquisition and working mode transition of the Taiji-1 ESA in-orbit: (a) X-axis acquisition. (b) Y-axis acquisition. (c) Z-axis acquisition. (d) ϕ -attitude acquisition. (e) θ -attitude acquisition. (f) ψ -attitude acquisition.

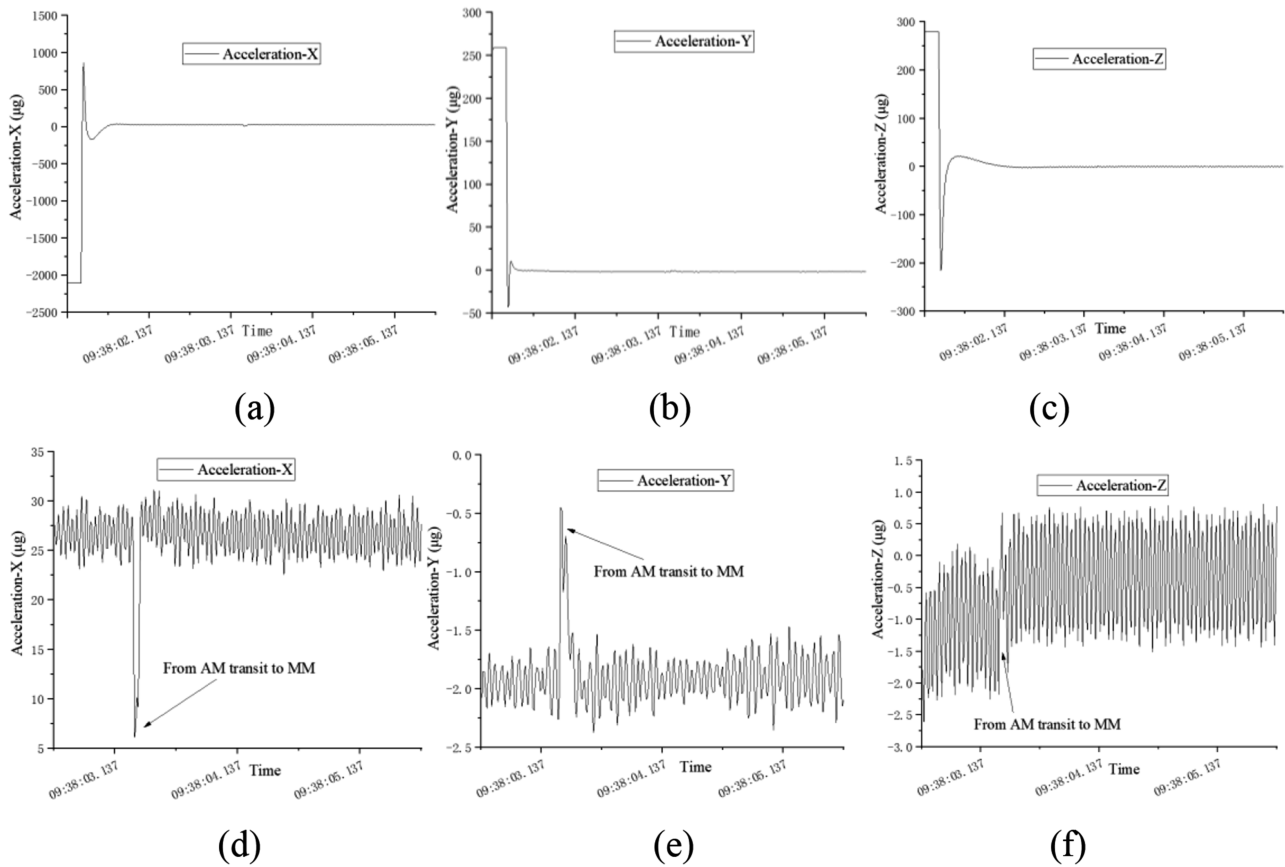


FIG. 11. Microgravity acceleration measured by the Taiji-1 ESA in-orbit: (a) X-axis acceleration. (b) Y-axis acceleration. (c) Z-axis acceleration. (d) X-axis acceleration after working mode transition. (e) Y-axis acceleration after working mode transition. (f) Z-axis acceleration after working mode transition.

measured formally. The microgravity acceleration onboard is given in Fig. 11.

According to the electrode parameters and electronic parameters of the sensitive axis and non-sensitive axis given in Table II, it can be analyzed that the natural resonance frequency ω_0 of the non-sensitive axis is about three times that of the sensitive axis, which means that the adjustment speed of the non-sensitive axis is faster. This can be clearly seen from the oscillation period of the sensing output and the feedback control output of the sensitive axis and non-sensitive axis during the acquisition process.

IV. CONCLUSION

By adjusting the amplitude of the carrier voltage, the detection gain switching of multiple sensing channels of the ESA can be easily achieved simultaneously and thus transition between AM and MM. It is reasonable and feasible to use the displacement sensing output as the criterion for transiting between AM and MM. The rationality of the design about working mode has been verified through the ground drop tower test and in-orbit flight tests of the Taiji-1 ESA.

In this paper, a dual-constraint criterion design of displacement sensing output and feedback control output is proposed for

transitioning between the MMLR and MMSR. This design has not been experimentally verified, which is limited by the free fall duration and microgravity level of the drop tower. In addition, it will be verified in the actual flight test in the future.

ACKNOWLEDGMENTS

The work described in this paper was funded by the National Key Research and Development Program of China (Grant No. 2021YFC2202401).

AUTHOR DECLARATIONS

Conflict of Interest

The authors have no conflicts to disclose.

Author Contributions

Zuolei Wang: Conceptualization (equal); Data curation (equal); Formal analysis (equal); Methodology (equal); Writing – original

draft (equal). **Yunpeng Li**: Conceptualization (equal); Data curation (equal); Methodology (equal); Software (equal); Validation (equal). **Jungang Lei**: Methodology (equal); Project administration (lead); Resources (equal); Supervision (equal); Validation (equal). **Zhenxing Wang**: Methodology (equal); Supervision (equal); Validation (equal). **Dongxue Xi**: Resources (equal); Validation (equal). **Jian Min**: Data curation (equal); Formal analysis (equal); Resources (equal). **Yongqiang Wei**: Resources (equal). **Shijia Yang**: Resources (equal); Validation (equal). **Ziren Luo**: Methodology (equal).

DATA AVAILABILITY

The data that support the findings of this study are available from the corresponding author upon reasonable request.

REFERENCES

- ¹R. Chhun, E. Hardy, M. Rodrigues *et al.*, “Microscope instrument in-flight characterization,” *Classical Quantum Gravity* **39**(20), 204005 (2022).
- ²T. Visser, E. N. Doornbos, C. C. de Visser *et al.*, “Torque model verification for the GOCE satellite,” *Adv. Space Res.* **62**(5), 1114–1136 (2018).
- ³W. Dong, W. Duan, W. Liu *et al.*, “Microgravity disturbance analysis on Chinese space laboratory,” *npj Microgravity* **5**, 18 (2019).
- ⁴J. Qiao, G. Xu, W. Liu *et al.*, “Comparison of Beidou autonomous navigation performance using the SRP model and onboard accelerometers,” *Acta Astronaut.* **173**, 183–194 (2020).
- ⁵N. Zahzam, B. Christophe, L. Vincent *et al.*, “Hybrid electrostatic–atomic accelerometer for future space gravity missions,” *Remote Sens.* **14**(14), 32373 (2022).
- ⁶D. Bortoluzzi, B. Foulon, C. García Marirrodriga, D. Lamarre *et al.*, “Object injection in geodesic conditions: In-flight and on-ground testing issues,” *Advances in Space Research* **45**(11), 1358–1379 (2010).
- ⁷E. J. Harrison, M. A. Meldrum, Z. Milburn *et al.*, “Development of a miniature electrostatic accelerometer (MESA) for low g applications summary report,” NASA Technical Reports BAC-60009-509, 1965.
- ⁸M. Rodrigues, J. Bergé, D. Boulanger *et al.*, “Space accelerometers for micro and nanosatellites: Fundamental physics and Geodesy missions from MICROSCOPE, GOCE and GFO return of experience,” in *The 4S Symposium 2022*, Vilamoura, Portugal, May 16–20, 2022.
- ⁹F. Liorzou, R. Chhun, and B. Foulon, “Ground based tests of ultra-sensitive accelerometers for space mission,” in *60th International Astronautical Congress*, IAC-09.A2.4.3, Daejeon, Republic of Korea, October 12–16, 2009.
- ¹⁰A. Allasio, A. Anselmi, G. Catastini *et al.*, “Goce mission: Design phases and in-flight experiences,” in *33rd Annual AAS Guidance and Control Conference*, Breckenridge, CO, USA, February 5–10, 2010.
- ¹¹B. Christophe, B. Foulon, and F. Liorzou, “Status of development of the future accelerometers for next generation gravity missions,” in *International Symposium on Advancing Geodesy in a Changing World*, Kobe, Japan, July 30–August 4, 2017.
- ¹²F. Liorzou, P. Touboul, M. Rodrigues *et al.*, “MICROSCOPE instrument description and validation,” *Classical Quantum Gravity* **39**(20), 204002 (2022).
- ¹³P. Touboul, G. Métris, and H. Sélég, “Gravitation and Geodesy with inertial sensors, from ground to space,” *Aerosp. Lab* **12**, 1–16 (2016).
- ¹⁴Y.-L. Wu, Z.-R. Luo, J.-Y. Wang *et al.*, “China’s first step towards probing the expanding universe and the nature of gravity using a space borne gravitational wave antenna,” *Commun. Phys.* **4**, 34 (2021).
- ¹⁵L. Lafargue, “Configuration mécanique d’accéléromètres électrostatiques pour le test en orbite du principe d’équivalence,” Ph.D. thesis, University of Paris VI, 2002.
- ¹⁶Z. Xiaoqian, Y. Longgen, W. Wendong *et al.*, “Some key technics of drop tower experiment device of National Microgravity Laboratory (China) (NMLC),” *Sci. China, Ser. E: Eng. Mater. Sci.* **48**(3), 305–316 (2005).